CrossMark

# First-Principles Study on the Stability and STM Image of Borophene

Zhifen Luo, Xiaoli Fan* and Yurong An

## Abstract

Very recently, borophene (atomic-thin two-dimensional boron sheet) has been successfully synthesized on the Ag(111) surface by deposition. Two kinds of structures were found. However, the identification of the monolayer boron sheets grown on the metal substrate, as well as the stability of different 2D boron sheets, is controversial. By performing the first-principles calculations, present study investigates the atomic structure, stability, and electronic properties of the most possible boron sheets grown on metal surface, namely, buckled triangular, $\beta_{12}$, and $\chi_3$ types of crystal lattice. Our result shows that all the three freestanding sheets are thermodynamically unstable and all are metallic. On the other hand, our result indicates the Ag(111) substrate stabilize these sheets. Additionally, our simulated STM images of these monoatomic-thin boron sheets on Ag(111) surface reproduce the experiment observations well and clearly identify the as-grown boron sheets.

**Keywords:** Atomic-thin boron sheet, First-principles calculations, Atomic structure, Stability, STM image

## Background

Since the discovery of graphene, two-dimensional (2D) materials have become one of the most active nanomaterials due to their unique physical properties and potential applications in next-generation electronics and energy conversion device [1–7]. Recently, a class of 2D boron nanostructures has been discovered and attracted significant attentions [8–21]. However, there was no evidence that the 2D boron sheets could be realized experimentally until very recently, both Mannix et al. [22] and Feng et al. [23] made spectacular advances in realizing experimentally the atomic-thin 2D boron sheets. The extended 2D boron sheet is called "borophene", in analogy to graphene.

During the last two decades, numerous 2D boron nanostructures have been discovered [8–21]. Besides the hexagonal sheet and the triangular sheet [20, 21], as well as the buckled triangular sheets [8], other 2D boron sheets with hexagonal holes, like the $\alpha$-sheet [9, 18], $\beta$-sheet [9, 18], $\gamma$-sheet [19], and g1/8 and g2/15 sheets [15], were examined by the ab initio calculations. It was suggested that the triangular planar boron lattice with hexagonal vacancies is more stable [9]. And a variety of such triangular boron layer with different patterns of hexagonal holes were reported by both the computational and experimental research groups [11, 13–16]. However, all of these monoatomic-thin boron layers are higher in energy than boron's three-dimensional (3D) bulk state, which means that the 2D structure of boron is disadvantaged thermodynamically. Thus, a sufficiently "sticky" substrate is necessary to suppress the 3D nucleation barrier to entice the atoms into the 2D route.

Recently, the formation of boron sheets on metal and metal boride substrates has been explored by first-principles calculations [24]; it suggests that the boron sheets can be grown on the Ag(111) and Au(111) surface. Additionally, Piazza et al.'s [14] study provide experimental evidence that the monolayer boron sheets are achievable based on their observations of $B_{36}$ cluster; it was shown to be a highly stable planar cluster with a central hexagonal hole [14]. More recently, two groups [22, 23] successfully synthesized the atomic-thin, crystalline 2D boron sheets on a silver surface by directly evaporating a pure boron source via molecular beam epitaxy.

Mannix et al. [22] found two distinct phases of the boron sheet on silver substrate using high-resolution scanning tunneling microscopy (STM) characterization: a striped phase and a homogeneous phase. Feng et al.

* Correspondence: xlfan@nwpu.edu.cn
State Key Laboratory of Solidification Processing, School of Material Science and Engineering, Northwestern Polytechnical University, 127 YouYi Western Road, Xi'an, Shaanxi 710072, China

Luo *et al. Nanoscale Research Letters* (2017) 12:514

Page 2 of 8

[23] also found two phases of boron sheet, which look quite similar to those reported in Mannix et al.'s report, and they described the homogeneous phase with zigzag rows of protrusions as $\chi_3$ lattice of boron sheet. On the other hand, their interpretations for the stripe phase are quite different. Mannix et al. [22] assigned the striped phase as a buckled triangular lattice without vacancy. But Feng et al. [23] proposed the stripe phase to be the rectangular lattice displaying parallel rows of hexagonal holes, which was known as the $\beta_{12}$ sheet.

The exact configurations and properties, as well as the applications of these 2D boron sheets, have attracted tremendous attentions [19, 22, 24, 25]. It was reported that the buckled triangular borophene is a highly anisotropic metal with a high Young modulus along its armchair direction which exceeds that of graphene [22]. Sun et al. also found that the lattice thermal conductivity of the buckled triangular borophene is strongly anisotropic [26]. Moreover, Gao et al. reported that the $\beta_{12}$ borophene and $\chi_3$ borophene may be another superconducting phase of boron besides $MgB_2$ thin film [27]. However, the thermodynamic stability of $\beta_{12}$ borophene and $\chi_3$ borophene are controversial [27, 28]. According to Gao et al.'s study, both $\beta_{12}$ borophene and $\chi_3$ borophene are stable [27]. But Penev et al. reported that both $\beta_{12}$ borophene and $\chi_3$ borophene have imaginary frequencies near the G point in their phonon spectrums [28].

To provide a better understanding for the experimental achievable borophene, we systematically investigated the possible atomic structures and their stability, as well as the electronic properties by performing the first-principles calculations. Our results indicate that $\beta_{12}$ and $\chi_3$ sheets are thermodynamically unstable. Additionally, the configurations of buckled triangular, $\beta_{12}$, and $\chi_3$ sheets all show metallic feature. Moreover, we have simulated the STM images for the freestanding and epitaxial monolayer of boron on the Ag(111) surface; we found buckled triangular and $\beta_{12}$ boron sheets on Ag(111) surface both look as stripe phases but with little difference.

## Computational Methods

The calculations are performed by using the Vienna abinitio simulation package (VASP) based on density functional theory (DFT) [29, 30]. The projector-augmented-wave method was adopted for the calculations of electron–ion interactions [31, 32]. And the electronic exchange–correlation interactions were described by the generalized gradient approximation (GGA) using the Perdew–Burke–Ernzerhof (PBE) functional [33]. Wave functions were expanded in a plane wave basis with an energy cutoff of 500 eV. The first Brillion zone were sampled by 25 × 15 × 1, 15 × 9 × 1, and 11 × 11 × 1 k-mesh for the buckled triangular, $\beta_{12}$, and $\chi_3$ phases of borophene, respectively. To simulate the 2D boron

sheets, a vacuum space of at least 20 Å is included along the Z direction to minimize the interaction between the periodic images. The convergence criterion was set to $10^{-5}$ eV between two ionic steps for the self-consistency process. All structures were fully relaxed until the force on each atom was less than 0.02 eV $Å^{-1}$, and the bottom two layers of silver atoms were fixed. Phonon dispersion spectrums have been computed by using the finite displacement method as implemented in the PHONOPY package [34].

The STM images were simulated using the Tersoff–Hamann formula and its extension [35]. Briefly, assuming that the density of states of the tip is constant, we can approximate the STM tunneling current with the local density of states, $\rho(\overrightarrow{r}, E)$, as the only variable with the following expression:

$$I(V) \propto \int_{E_F}^{E_F + eV} \rho(\overrightarrow{r}, E) dE$$

$$\rho(\overrightarrow{r}, E) = \sum_i \left| \psi_i(\overrightarrow{r})^2 \right| \delta(E - E_i)$$

where $\rho(\overrightarrow{r}, E)$ is the LDOS on the sample surface, $\psi_i(\overrightarrow{r})$ is the sample wave function with energy $E_i$, and $E_F$ is the Fermi energy. When the states in $\rho(\overrightarrow{r}, E)$ are filled, it is also common to refer to $\rho(\overrightarrow{r}, E)$ as the charge density of the states. The simulated STM images were obtained using the constant current mode based on calculated electron densities.

## Results and Discussion

Figure 1 shows our calculated results for the buckled triangular, $\beta_{12}$, and $\chi_3$ lattice structures of borophene. Unlike the one-atom thin and planar hexagonal configuration of graphene, buckled triangular borophene shows buckling along one lattice direction. On the other hand, the structures of $\beta_{12}$ and $\chi_3$ borophenes are planar without out-of-plane buckling. Figure 1a shows that there are two boron atoms in the unit cell of buckled triangular borophene. And the space group of buckled triangular borophene is Pmmn. Our optimized lattice constants are $a = 1.613$ Å and $b = 2.866$ Å, agreeing well with previous theoretical and experimental results [22]. The $\beta_{12}$ borophene shown in Fig. 1b has filled and empty hexagons along the zigzag direction; the corresponding space group is P2mm. There are five boron atoms in the unit cell. The lattice constants are 2.916 and 5.075 Å along the $a$ and $b$ directions. The unit cell of $\chi_3$ borophene is rhombic, having four boron atoms and the lattice constant of 4.448 Å. Its space group is C2mm. Table 1 lists our calculation results on the lattice constants, which agree well with previous results [22, 23, 27, 36].
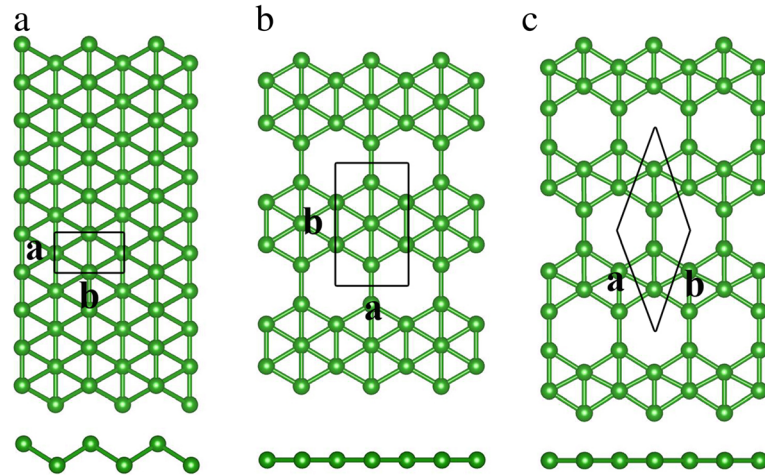
**Fig. 1** Top and side views of buckled triangular (**a**), $\beta_{12}$ (**b**), and $\chi_3$ (**c**) boron sheets. The green balls represent the boron atoms. The rectangles and rhombus enclosed by solid black lines denote the unit cells. The letters *a* and *b* represent the lattice parameter

As shown in Fig. 1, there are vacancies in both $\beta_{12}$ and $\chi_3$ sheets but not in the buckled triangular lattice and the number of vacancies in $\beta_{12}$ and $\chi_3$ borophene is different. The vacancy concentration $\eta$ is defined as the ratio between the number of vacancy sites and total sites (including vacancy) in the unit cell; it is a quantity describing the boron sheets from global and local points of view [9]. $\eta$ is 1/6 in $\beta_{12}$ lattice and 1/5 in $\chi_3$ lattice. Compared to the $\beta_{12}$ lattice, Fig. 1c shows that the neighboring vacancy rows in $\chi_3$ borophene are shifted by half of the lattice constant in zigzag direction, resulting in a planar of C2mm symmetry.

We calculate the average energy of each boron atom using the following equation for the three structures and use it to compare the relative stability of the three structures; this method has been applied in Ref. [23]

$$E_{\mathrm{FB}} = E_{\mathrm{borophene}}/n$$

where $E_{\mathrm{borophene}}$ and $n$ are the energy and the number of boron atoms in one unit cell, respectively. Our calculated results are summarized in Table 2. It indicates that the $\beta_{12}$ phase is the most stable, while the $\chi_3$ phase is the least stable with relative higher energy of 0.08 eV.

We then calculated the phonon dispersion spectrum for the three phases of buckled triangular, $\beta_{12}$, and $\chi_3$

borophene. Figure 2 shows the phonon dispersion spectrums along the high symmetry directions. As shown in Fig. 2a, there are three acoustic and three optical phonon branches for the buckled triangular borophene. It also shows imaginary values near the G point along the X–G direction, indicating that the lattice is unstable along the *a* direction, which explains the stripe formed along the *a* direction in the experimental STM images [23]. In fact, recent studies have suggested that the biaxial tensile and uniaxial tensile cannot stabilize the freestanding buckled triangular borophene even under the tensile stress of 0.08% [36, 37]. Figure 2b, c shows that there are also imaginary frequencies near the G point of $\beta_{12}$ and $\chi_3$ phases. Our results show that all the three phases of buckled triangular, $\beta_{12}$, and $\chi_3$ are unstable.

We further studied the electronic structures of buckled triangular borophene, $\beta_{12}$ borophene, and $\chi_3$ borophene. The calculated band structures along the high-symmetry directions are shown in Fig. 3. As shown in Fig. 3, all the three phases of buckled triangular, $\beta_{12}$, and $\chi_3$ borophenes are metallic. Particularly, for the buckled triangular borophene as shown in Fig. 3a, three energy bands cross the Fermi level: one is along the S–Y direction and the other two are along the G–X direction. However, we have mentioned in the above sections that the buckled triangular is buckling along the *b* direction, which opens a bandgap of

**Table 1** Our calculated lattice constants *a*, *b*, and *γ* for the buckled triangular, $\beta_{12}$ and $\chi_3$ boron sheets. Previous results are also listed for comparison

|  | Previous studies | | | Present result | | |
|---|---|---|---|---|---|---|
|  | *a* (Å) | *b* (Å) | *γ* | *a* (Å) | *b* (Å) | *γ* |
| b$_\triangle$ | 1.617 [22] | 2.872 [22] | 90° | 1.613 | 2.866 | 90° |
| $\beta_{12}$ | 2.922 [23] | 5.057 [23] | 90° | 2.916 | 5.075 | 90° |
| $\chi_3$ | 4.443 [27] | 4.443 [27] | 38.173° [27] | 4.448 | 4.448 | 38.182° |

**Table 2** Average energy for boron atoms in the freestanding ($E_{\mathrm{FB}}$) and epitaxial ($E_{\mathrm{EB}}$) boron sheets on the Ag(111)

|  | Previous studies | | | Present result | | | |
|---|---|---|---|---|---|---|---|
|  | b$_\triangle$ | $\beta_{12}$ | $\chi_3$ | b$_\triangle$ | $\beta_{12}$ | $\chi_3$ | $\chi_3{'}$ |
| $E_{\mathrm{FB}}$(eV/atom) | / | −6.23 [23] | −6.19 [23] | −6.19 | −6.23 | −6.15 | −6.15 |
| $E_{\mathrm{EB}}$(eV/atom) | / | −6.32 [23] | −6.35 [23] | −6.29 | −6.33 | −6.32 | −6.35 |

The results for the buckled triangular, $\beta_{12}$, and $\chi_3$ boron sheets are listed

Luo *et al. Nanoscale Research Letters* (2017) 12:514

Page 4 of 8
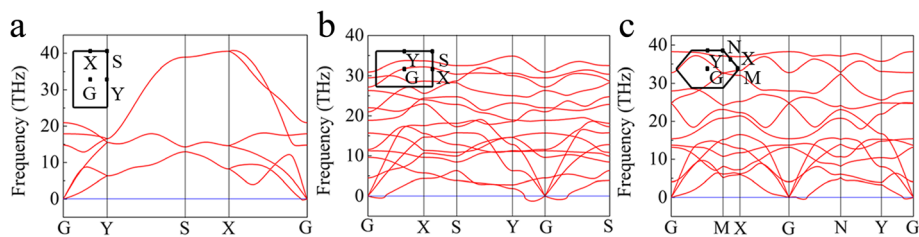


**Fig. 2** The phonon dispersion of the **a** buckled triangular, **b** $\beta_{12}$, and **c** $\chi_3$ boron sheets. The high symmetry points are shown on the left corner

9.63 and 4.32 eV along the X–S and Y–G directions, respectively. It indicates that the buckled triangular borophene behaves as a metal with strong anisotropy and the electrical conductivity is confined along the uncorrugated *a* direction.

Additionally, we studied the atomic structures and stability of the buckled triangular, $\beta_{12}$, and $\chi_3$ boron sheets on the Ag(111) substrate. The results are shown in Fig. 4. The unit cell of buckled triangular borophene on Ag(111) surface is the (1 × 3) supercell of freestanding buckled triangular borophene and the rectangular 1 × ($\sqrt{3}$)R30° supercell of the Ag(111) substrate. For the configuration of $\beta_{12}$ sheet on the Ag(111) surface, the unit cell is the unit cell of $\beta_{12}$ borophene and 1 × ($\sqrt{3}$)R30° supercell of the Ag(111) surface. Our calculations show that the $\beta_{12}$ borophene matches to Ag(111) surface (~ 1% mismatch) better than the buckled triangular borophene (~ 3% mismatch). The $\chi_3$ borophene forms two configurations on the Ag(111) surface, as shown in Fig. 4c, d, which are named as $\chi_3$ and $\chi_3$'. The unit cell of $\chi_3$ is rhombus with lattice constant of $a$ = 8.67 Å, and the unit cell of $\chi_3$' is orthorhombic with lattice parameters of $a$ = 2.89 Å and $b$ = 25.02 Å; it is the 1 × (5$\sqrt{3}$)R30° supercell of the Ag(111) surface.

According to our calculations, the vertical distances from the Ag(111) surface to the lower and upper boron atomic layers of the buckled triangular borophene are 2.5 and 3.3 Å, respectively, indicating the weak interaction between the boron sheet and the Ag substrate. The $\beta_{12}$, $\chi_3$, and $\chi_3$' sheets all remain planar on the Ag(111) surface, and the vertical distances between the boron sheet and the Ag surface are 2.4~2.9 Å. The results agree with

the measured thickness of ~ 2.7 to 3.1 Å reported by Mannix et al. [22]. We compared the atomic structures of buckled triangular, $\beta_{12}$, $\chi_3$, and $\chi_3$' phases of borophene on Ag substrate with the counterparts of the freestanding borophene and found that these four structures change little. The buckling height $h$ of buckled triangular borophene is shorter from 0.910 to 0.857 Å, and the B-B lengths are longer about 0.1 Å. Moreover, the hexagon vacancies in the $\beta_{12}$ borophene shrink along a direction, and those in $\chi_3$ borophene become little larger.

Similar to the calculation for the relative stability of the freestanding borophene, we further calculated the average energy of each boron atom for the boron sheets on the Ag(111) surface via the following formula:

$$E_{EB} = \frac{1}{n}(E_{tot} - E_{sub})$$

where $E_{tot}$ is the total energy of the boron sheet and the Ag(111) surface, $E_{sub}$ is the energy of Ag substrate, and $n$ is the number of boron atoms in one unit cell. Our result shows that the possibility of forming buckled triangular, $\beta_{12}$, $\chi_3$, and $\chi_3$' lattices on the Ag(111) surface is similar based on their close energies. Additionally, the energies of the borophene on the Ag(111) surface are lower by 0.1~0.2 eV per boron atom relative to the freestanding sheets. This means that Ag(111) surface stabilize the borophene.

Figure 5 shows our simulated STM images for the freestanding and as-grown boron sheets on Ag(111) surface, as well as the partial charge density for the freestanding boron sheets. As shown in Fig. 5a, the freestanding buckled triangular boron sheet features stripes of bright spots. Figure
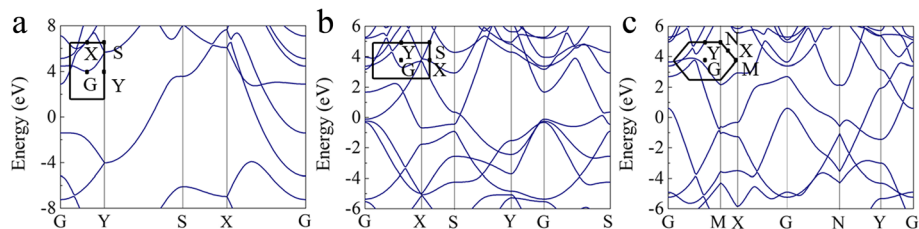


**Fig. 3** Calculated band structures for **a** buckled triangular, **b** $\beta_{12}$, and **c** $\chi_3$ boron sheets. The Fermi energy was set to zero. The high-symmetry points are shown on the left corner

Luo *et al. Nanoscale Research Letters* (2017) 12:514

Page 5 of 8
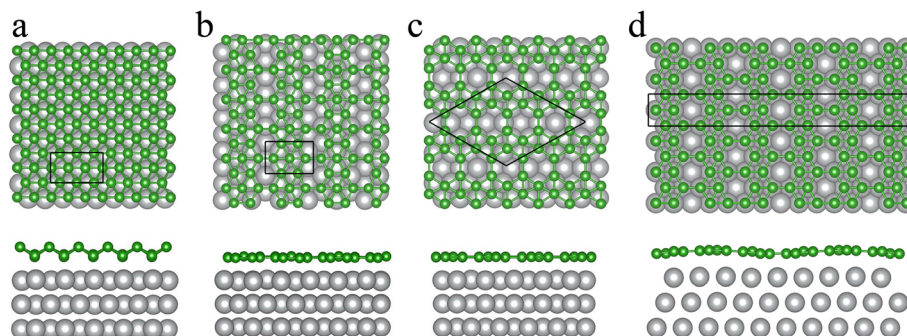


**Fig. 4** Top and side views of boron sheets on Ag(111) surface. **a** Buckled triangular, **b** $\beta_{12}$, **c** $\chi_3$, and **d** $\chi_3'$ boron sheet. The green and gray balls represent boron and silver atoms, respectively. The rectangles and rhombus enclosed by solid black lines denote the unit cells of boron sheets on the Ag(111) surface

5d indicates that the bright spots come from the $p_z$ orbit of upper boron atoms. Figure 5b shows rows of dark round spots surrounded by bright hexagons. Obviously, the hexagonal vacancies in $\beta_{12}$ lattice shown in Fig. 1b result in the dark spots, while the bright hexagons correspond to the $\sigma$ orbits of boron atoms around the hexagon holes as shown in Fig. 5e. As shown in Fig. 5c, the $\chi_3$ sheet displays rhombohedra pattern of bright spots in dumbbell shape. These bright dumbbell spots actually are the $p_z$ orbits of the two boron atoms and the $\sigma$ orbits formed between them.

The boron sheets on the Ag substrate all have larger unit patterns relative to the freestanding ones because of the mismatches between the unit cells of borophene and Ag(111) surface. Figure 5g shows our simulated STM image for buckled triangular boron sheet on Ag(111) surface. It displays stripes of bright spots in spindle shape, which agree very well with experimental observations [22]. Comparing with the image of freestanding buckled triangular boron sheet shown in Fig. 5a, the unit cell of STM image of buckled triangular boron sheet on the Ag(111) surface increases to three times. And the shape changes to spindle from round. The STM image of $\beta_{12}$ sheet on Ag(111) surface shown in Fig. 5h shows rows of dark oval spots surrounded by four bright spots on its four corners. Different from the
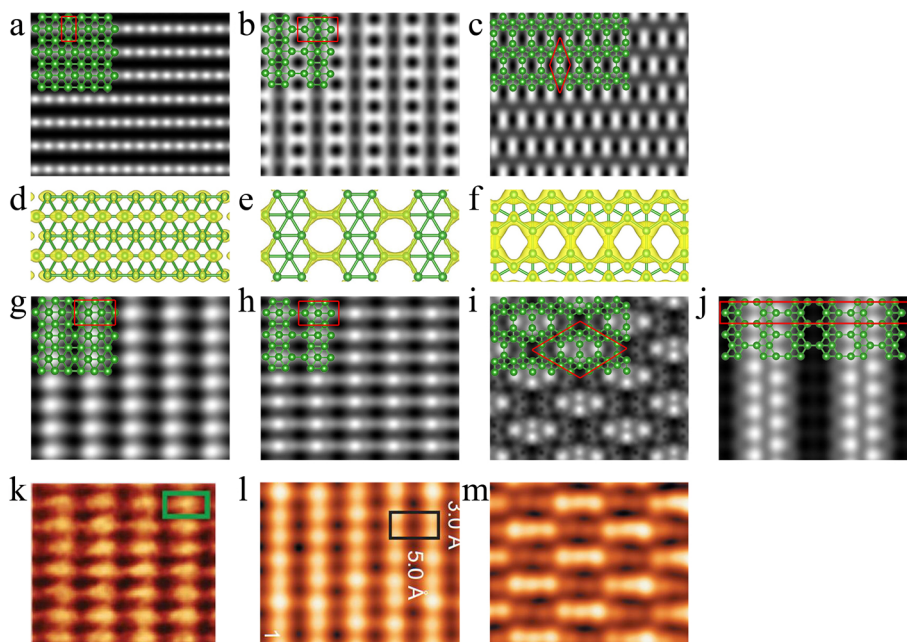


**Fig. 5** Simulated STM images of freestanding and epitaxial boron sheets on Ag(111) surface. Freestanding **a** triangular, **b** $\beta_{12}$, and **c** $\chi_3$ boron sheets. Partial charge density of freestanding **d** triangular, **e** $\beta_{12}$, and **f** $\chi_3$ boron sheets. **g** Buckled triangular, **h** $\beta_{12}$, **i** $\chi_3$, and **j** $\chi_3'$ boron sheet on the Ag(111) surface. The bias voltage is 1.0 V. The green balls represent the boron atoms. The rectangles and rhombus enclosed by solid red lines denote the unit cells of freestanding and as-grown boron sheets on Ag(111) surface, respectively. Experimentally observed **k** stripe phase in Ref. [22], **l** stripe phase in Ref. [23], and **m** homogeneous phase in Ref. [23]

Luo *et al. Nanoscale Research Letters* (2017) 12:514

Page 6 of 8

image of freestanding $\beta_{12}$ sheet shown in Fig. 5b, the bright spots come from the $p_z$ orbits of the boron atoms in the center of hexagons. As shown in Fig. 5i, the $\chi_3$ sheet has a rhombohedra STM pattern which is in good agreement with the experimental observed S2 phase [23]. The group of bright spots in the rhombohedra unit cell corresponds to the $\sigma$ orbits and $p_z$ orbits of the higher boron atoms in the unit cell, while the other boron atoms are invisible because they are lower.

Mannix et al. [22] and Feng et al. [23] both reported the stripe phase for 2D boron sheets on the Ag(111) surface based on their STM observations, and both the STM images feature parallel rows of protrusions. However, the shape of the bright spots in the two experimental observations is different; they are spindle in Mannix et al.'s report [22] and oval in Feng et al.'s [23]. Our simulated STM images of buckled triangular and $\beta_{12}$ boron sheets match very well with the experimental observed stripe phases in Ref. [22] and Ref. [23], respectively, and the images shown in Fig. 5g, h clearly reproduce the difference between the experimental observations of Mannix et al. [22] and Feng et al. [23]. It also provides us a way to distinguish the two lattice of buckled triangular and $\beta_{12}$. As for the STM image of $\chi_3$ sheet on the Ag(111) surface, as shown in Fig. 5i, it agrees with the experimental observation [23], but our result indicates

that the bright spots come from the boron atoms on the edge of hexagonal vacancies instead of the filled triangular area as indicated in Ref. [23].

In order to further distinguish the lattice structures of boron sheets on the Ag(111) surface, we simulated the STM images of boron sheet on Ag(111) at several different bias voltage. As shown in Fig. 6, the simulated STM images for the buckled triangular borophene display stripes of bright spots in spindle shape at positive voltage. But at the negative bias voltage of − 0.4 V, the simulated STM images show the light and dark stripes, which matches well with experiment result [22]. On the other hand, the simulated STM images of $\beta_{12}$ borophene maintain the oval shape at both the positive and negative bias voltage. Hence, buckled triangular structure is more likely to be the correct configuration of stripe phase. As for the STM image of $\chi_3$ borophene, Fig. 6 indicates that the bright spots in all the images come from the boron atoms at the edge of hexagonal vacancies, but their bright contrast changes as the voltage changes from positive to negative. As the bias voltage of 0.2 and − 0.4 V, the brightness of the spots are similar. Additionally, our simulated STM images for the $\chi_3$' configuration look similar at bias voltage from 0.8 to − 1.0 V (Fig. 6). They all show the bright spots coming from the boron atoms on the edge of hexagonal vacancies, but only the
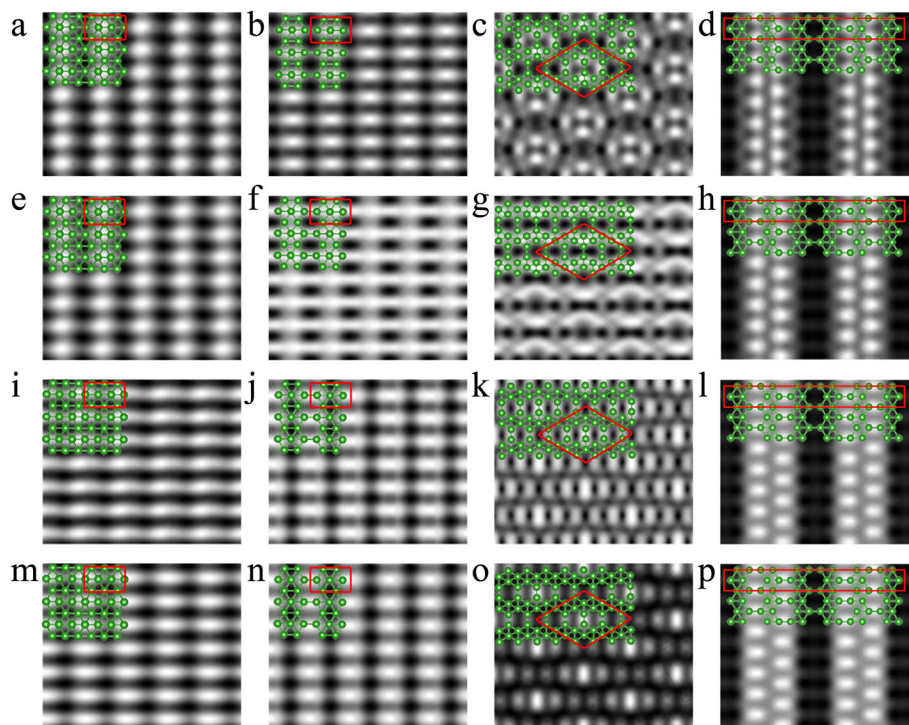


**Fig. 6** Simulated STM images for boron sheets on Ag(111). Buckled triangular borophene on Ag(111) at **a** 0.8, **e** 0.2, **i** − 0.4, and **m** − 1.0 V. $\beta_{12}$ borophene on Ag(111) at **b** 0.8, **f** 0.2, **j** − 0.4, and **n** − 1.0 V. $\chi_3$ borophene on Ag(111) at **c** 0.8, **g** 0.2, **k** − 0.4, and **o** − 1.0 V. $\chi_3$' borophene on Ag(111) at **d** 0.8, **h** 0.2, **l** − 0.4, and **p** − 1.0 V. The green balls represent the boron atoms. The rectangles and rhombus enclosed by solid red lines denote the unit cells of as-grown boron sheets on Ag(111) surface

Luo et al. Nanoscale Research Letters (2017) 12:514

Page 7 of 8

higher boron atoms are visible and the lower boron atoms in the middle of the unit cell are invisible.

## Conclusions

In summary, we performed first-principles calculations on the atomic structure, stability, and electronic property for the three 2D boron sheets which were grown on the metal surface very recently, namely, buckled triangular, $\beta_{12}$, and $\chi_3$ lattice. Our calculations indicate that all the three boron sheets are thermodynamically unstable without the support of metal substrate. The band structures indicate that the buckled triangular boron sheet behaves as a metal with strong anisotropy and $\beta_{12}$ and $\chi_3$ boron sheets are also metallic without energy gaps. Additionally, our results show that the energies for the three types of lattices are very close and the lattice match between the buckled triangular and $\beta_{12}$ boron sheets and Ag(111) surface is quite small. Furthermore, we have found that both buckled triangular and $\beta_{12}$ boron sheets on the Ag(111) form the rectangular lattice and the parallel striped patterns of STM image but with little difference. Our results provide details to distinguish the two lattices. Most importantly, our simulated STM images give a new explanation to the experimentally observed boron sheets on the Ag(111) surface.

### Abbreviations
2D: Two-dimensional; 3D: Three-dimensional; STM: Scanning tunneling microscopy

### Authors' Contributions
ZFL designed the study and performed the research. ZFL and XLF led the data discussion and interpretation. The manuscript was drafted by ZFL and XLF but was read and approved by all authors. YRA participated in performing research and helped to draft the manuscript. All authors read and approved the final manuscript.

### Competing Interests
The authors declare that they have no competing interests.

## Publisher's Note
Springer Nature remains neutral with regard to jurisdictional claims in published maps and institutional affiliations.

### References
1. Novoselov KS, Fal'ko VI, Colombo L, Gellert PR, Schwab MG, Kim K (2012) A roadmap for graphene. Nature 490:192–200
2. Xu M, Liang T, Shi MM, Chen HZ (2013) Graphene-like two-dimensional materials. Chem Rev 113:3766–3798
3. Balendhran S, Walia S, Nili H, Sriram S, Bhaskaran M (2015) Graphene analogues: elemental analogues of graphene: silicene, germanene, stanene, and phosphorene. Small 11:640–652
4. Ferrari AC, Bonaccorso F, Fal'Ko V, Novoselov KS, Roche S, Bøggild P, Borini S, Koppens FHL, Palermo V, Pugno N (2015) Science and technology roadmap for graphene, related two-dimensional crystals, and hybrid systems. Nano 7:4598
5. Johari P, Shenoy VB (2012) Tuning the electronic properties of semiconducting transition metal dichalcogenides by applying mechanical strains. ACS Nano 6:5449–5456
6. Klinovaja J, Loss D (2013) Spintronics in MoS$_2$ monolayer quantum wires. Phys Rev B 88:4049–4057
7. Xu Y, Gan ZX, Zhang SC (2014) Enhanced thermoelectric performance and anomalous seebeck effects in topological insulators. Phys Rev Lett 112:770–777
8. Kunstmann J, Quandt A (2006) Broad boron sheets and boron nanotubes: an ab initio study of structural, electronic, and mechanical properties. Phys Rev B 74:035413
9. Tang H, Ismailbeigi S (2007) Novel precursors for boron nanotubes: the competition of two-center and three-center bonding. Phys Rev Lett 99: 115501
10. Tang H, Ismailbeigi S (2009) Self-doping in boron sheets from first principles: a route to structural design of metal boride nanostructures. Phys Rev B Condens Matter 80:134113
11. Li WL, Zhao YF, Hu HS, Li J, Wang LS (2014) [B$_{30}$]$^-$: a quasiplanar chiral boron cluster. Angew Chem 126:5646–5651
12. Zhou XF, Dong X, Oganov AR, Zhu Q, Tian Y, Wang HT (2014) Semimetallic two-dimensional boron allotrope with massless Dirac fermions. Phys Rev Lett 112:085502
13. Li WL, Chen Q, Tian WJ, Bai H, Zhao YF, Hu HS, Li J, Zhai HJ, Li SD, Wang LS (2014) The B$_{35}$ cluster with a double-hexagonal vacancy: a new and more flexible structural motif for borophene. J Am Chem Soc 136:12257–12260
14. Piazza ZA, Hu HS, Li WL, Zhao YF, Li J, Wang LS (2014) Planar hexagonal B$_{36}$ as a potential basis for extended single-atom layer boron sheets. Nat Commun 5:3113
15. Penev ES, Bhowmick S, Sadrzadeh A, Yakobson BI (2012) Polymorphism of two-dimensional boron. Nano Lett 12:2441–2445
16. Wu XJ, Dai J, Zhao Y, Zhuo ZW, Yang JL, Zeng XC (2012) Two-dimensional boron monolayer sheets. ACS Nano 6:7443–7453
17. Zhou XF, Artem RO, Wang ZH, Ivan AP, Alexander IB, Wang HT (2016) Two-dimensional magnetic boron. Phys Rev B 93:085406
18. Tang H, Ismailbeigi S (2010) First-principles study of boron sheets and nanotubes. Phys Rev B 82:115412
19. Özdoğan C, Mukhopadhyay S, Hayami W, Guvenc ZB, Pandey R, Boustani I (2010) The unusually stable B$_{100}$ fullerene, structural transitions in boron nanostructures, and a comparative study of α- and γ-boron and sheets. J Phys Chem C 114:4362–4375
20. Boustani I, Quandt A, Hernandez E, Rubio A (1999) New boron based nanostructured materials. J Chem Phys 110:3176
21. Evans MH, Joannopoulos JD, Pantelides ST (2005) Electronic and mechanical properties of planar and tubular boron structures. Phys Rev B 72:045434
22. Mannix AJ, Zhou XF, Kiraly B, Wood JD, Alducin D, Myers BD, Liu X, Fisher BL, Santiago U, Guest JR, Yacaman MJ, Ponce A, Oganov AR, Hersam MC, Guisinger NP (2015) Synthesis of borophenes: anisotropic, two-dimensional boron polymorph. Science 350:1513
23. Feng B, Zhang J, Zhong Q, Li W, Li S, Li H, Cheng P, Meng S, Chen L, Wu K (2016) Experimental realization of two-dimensional boron sheets. Nat Chem 8:563
24. Liu YY, Penev ES, Yakobson BI (2013) Probing synthesis of two-dimensional boron by first-principles computations. Angew Chem Int Edit 52:3156–3159
25. Liu HS, Gao JF, Zhao JJ (2013) From boron cluster to two-dimensional boron sheet on Cu(111) surface: growth mechanism and hole formation. Sci Rep 3:3238
26. Sun H, Li Q, Wan XG (2016) First-principles study of thermal properties of borophene. Phys Chem Chem Phys 18:14927–14932
27. Gao M, Li QZ, Yan XW, Wang J (2017) Prediction of phonon-mediated superconductivity in borophene. Phys Rev B 95:024505
28. Penev ES, Kutana A, Yakobson BI (2016) Can two-dimensional boron superconduct. Nano Lett 16:2522–2526
29. Kresse G, Furthmuller J (1996) Efficient iterative schemes for ab initio total-energy calculations using a plane-wave basis set. Phys Rev B: Condens Matter Mater Phys 54:11169–11186

Luo *et al. Nanoscale Research Letters* (2017) 12:514

Page 8 of 8

30. Kresse G, Furthmuller J (1996) Efficiency of ab-initio total energy calculations for metals and semiconductors using a plane-wave basis set. Comput Mater Sci 6:15–50

31. Kresse G, Joubert D (1999) From ultrasoft pseudopotentials to the projector augmented-wave method. Phys Rev B 59:1758–1775

32. Blöchl PE (1994) Projector augmented-wave method. Phys Rev B 50: 17953–17979

33. Perdew JP, Burke K, Ernzerhof M (1996) Generalized gradient approximation made simple. Phys Rev Lett 77:3865–3868

34. Togo A, Tanaka I (2015) First principles phonon calculations in materials science. Scr Mater 108:1–5

35. Tersoff T, Hamann DR (1985) Theory of the scanning tunneling microscope. Phys Rev B 31:805

36. Wang H, Li Q, Gao Y, Miao F, Zhou XF, Wan XG (2016) Strain effects on borophene: ideal strength, negative Poisson's ratio and phonon instability. New J Phys 18:073016

37. Pang ZQ, Qian X, Yang RG, Wei YJ (2016) Super-stretchable borophene and its stability under strain. arXiv 1602:05370